Multimodal Electrothermal Silicon Microgrippers for Nanotube Manipulation

Nordström Andersen, Karin; Petersen, Dirch Hjorth; Carlson, Kenneth; Mølhave, Kristian; Sardan Sukas, Özlem; Horsewell, Andy; Eichhorn, Volkmar; Fatikow, S.; Bøggild, Peter

Published in:
IEEE Transactions on Nanotechnology

Link to article, DOI:
10.1109/TNANO.2008.2006558

Publication date:
2009

Document Version
Publisher's PDF, also known as Version of record

Multimodal Electrothermal Silicon Microgrippers for Nanotube Manipulation

Karin Nordström Andersen, D. H. Petersen, K. Carlson, K. Mølhave, Ozlem Sardan, A. Horsewell, Volkmar Eichhorn, Sergej Fatikow, *Member, IEEE*, and Peter Bøggild

***Abstract*—Microgrippers that are able to manipulate nanoobjects reproducibly are key components in 3-D nanomanipulation systems. We present here a monolithic electrothermal microgripper prepared by silicon microfabrication, and demonstrate pick-and-place of an as-grown carbon nanotube from a 2-D array onto a transmission electron microscopy grid, as a first step toward a reliable and precise pick-and-place process for carbon nanotubes.**

***Index Terms*—Carbon nanotubes, microgrippers, nanomanipulation, pick-and-place.**

I. Introduction

SEVERAL groups have previously used microfabrication to make microgrippers for manipulation [1], and commercial vendors exist today, such as Nascatec [2], Zyvex [3], and FemtoTools [4] . The concept of nanotweezers was first demonstrated by Kim and Lieber [5], who gripped nanowires and nanoparticles between two electrostatically biased carbon nanotubes attached to a glass capillary. Based on a simple five-electrode microcantilever layout similar to that of Kim *et al.* [1], submicron grippers were fabricated. These microgrippers were capable of both opening and closing without applying a voltage directly between the arms [6] and were used to manipulate silicon nanowires [7]. Here, we describe a more mechanically stable, electrothermal three-beam microgripper with a high gripping force, which can be fabricated in single-crystalline silicon (SCS) as well as polycrystalline silicon.

Manipulation of a carbon nanotube (CNT) from one place to another can be done inside a scanning electron microscope (SEM), in which a suitable combination of visual resolution and sample space allows macroscale manipulators with micro- or nanoscale precision to be incorporated, yet monitored with nanometer-scale precision [8]–[11]. Complex multiprobe systems, allowing two or more scanning probe tips to be moved independently inside a SEM, have been used to characterize the mechanical properties of nanotubes and nanowires [3]. In these experiments, a combination of surface forces acting between the tip and the nanotube, a local soldering or gluing induced by electron beam deposition of carbonaceous material, and mechanical force applied to the nanotube by two individual tips, was used for pick-and-place of the nanotube.

An array of vertically ordered CNTs [12] is an excellent example of a highly suited starting point for nanorobotic prototyping or even manufacturing of CNT-based devices.

One advantage of such a "component bank," with well-defined positions for all the CNTs is that, once calibrated, the manipulation system can locate the CNT automatically. Another advantage is that the CNTs can be grown with a high degree of uniformity across a large area. A single CNT can then be picked up without risking sticking of other CNTs sticking to the manipulation tool [12]. In this context, a key problem is to provide a manipulation tool that is small and delicate enough to align to a sub-100-nm-diameter CNT, mechanically strong enough to detach the as-grown CNT from the surface, and able to release the CNT again at the desired target position.

Electrothermal actuators generally allow a relatively high gripping force to be combined with a compact design [13], while the design presented earlier [14] is capable of both opening and closing. This feature expands the deflection range and turns out to be convenient in actual experiments. For instance, in the event that the microgripper jaws remain closed due to adhesive material between the jaws—the "open" reaction is then often enough to force the gap open. In this paper, we show that by fabricating the microgripper in SCS $\langle 1\ 1\ 1 \rangle$ (see Fig. 1) as well as polycrystalline silicon, we obtain a similar actuation and gripping force as with Au [14], but with the added benefits of an easier fabrication process, less adhesion, and less out-of-plane bending. Finally, we demonstrate its use in manipulating carbon nanotubes.

II. Design Considerations

A. Actuation Modes

The 3-beam microgripper design allows several configurations for actuation of the microgrippers depending on how the bias voltage is applied over the six beams (see Fig. 2). To close the microgripper, the bias voltage V can be applied to the outer two beams with the inner four beams grounded, mode 3, $(V, 0, 0, 0, 0, V)$, or while letting the inner beams float [14], mode 2, $(V, 0, F, F, 0, V)$, where F refers to a floating potential, i.e. not connected. Biasing the left three beams with V and the

Manuscript received December 8, 2007; revised March 13, 2008. First published September 30, 2008; current version published January 16, 2009. This work was supported by the European Union under Grant NANOHAND (IP 034274) and Grant NANORAC (STREP 013680). The review of this paper was arranged by Associate Editor L. Dong.

K. N. Andersen, D. H. Petersen, K. Carlson, K. Mølhave, O. Sardan, and P. Bøggild are with MIC—Department of Micro and Nanotechnology, NanoDTU, Technical University of Denmark, DK-2800 Kongens Lyngby, Denmark (e-mail: kna@mic.dtu.dk; dhp@mic.dtu.dk; kenneth.carlson@mic.dtu.dk; krm@mic.dtu.dk; sar@mic.dtu.dk; boggild@mic.dtu.dk).

A. Horsewell is with IPL—Department of Manufacturing Engineering and Management, NanoDTU, Kemitorvet, DTU, DK-2800 Lyngby, Denmark (e-mail: horsewell@ipl.dtu.dk).

V. Eichhorn and S. Fatikow are with the Division of Microrobotics and Control Engineering, University of Oldenburg, 26111 Oldenburg, Germany.

Color versions of one or more of the figures in this paper are available online at http://ieeexplore.ieee.org.

Digital Object Identifier 10.1109/TNANO.2008.2006558

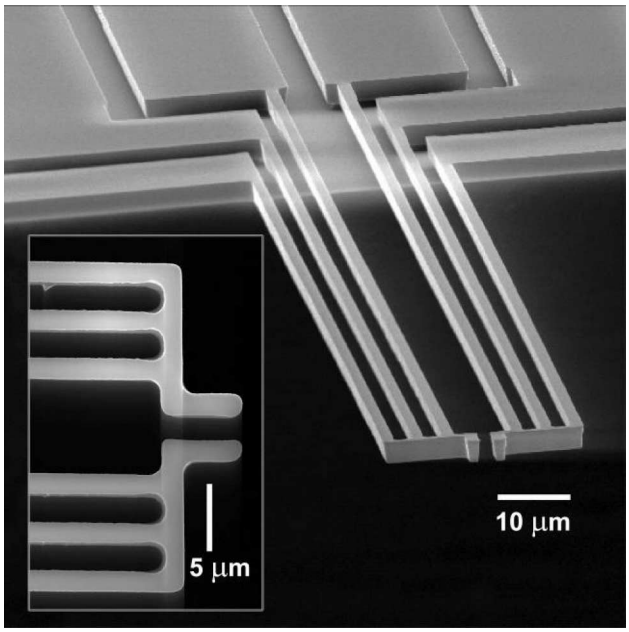

Fig. 1. SEM image of electrothermal three-beam microgrippers fabricated in SCS. The inset shows a magnified top view.

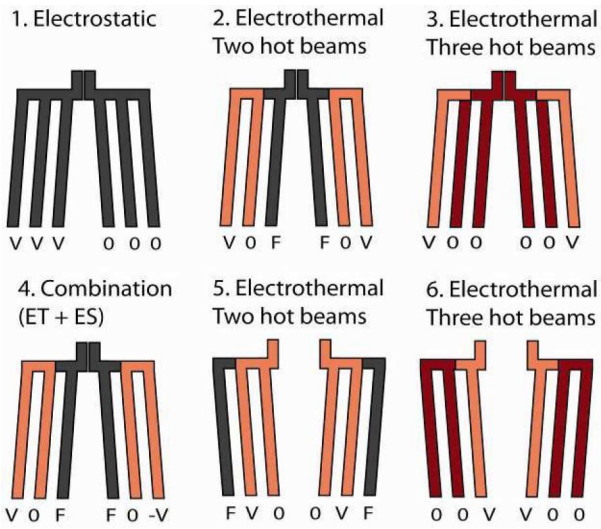

Fig. 2. Six different actuation modes of the three-beam microgripper. The connection configuration is shown below each illustration, i.e. with 0, V, and $-V$ signifying zero or finite potential, while F signifies "floating," not connected. (1) Electrostatic. (2) Electrothermal two hot beams. (3) Electrothermal three hot beams. (4) Combination (ET + ES). (5) Electrothermal two hot beams. (6) Electrothermal three hot beams.

right three with 0, mode 1, (V, V, V, 0, 0, 0), results in purely electrostatic actuation. Finally, the electrothermal and electrostatic actuation can be combined by using $(V, 0, F, F, 0, -V)$, where the different signs of the voltage on the left and right arms adds electrostatic to the electrothermal actuation.

Electrothermal actuation leads to high temperatures, ultimately reaching the melting point of silicon (~1700 K), as the maximum deflection is approached—this is a common problem for all electrothermal actuators. In addition, the three-beam actuator has its maximum temperature at the end-effector, which

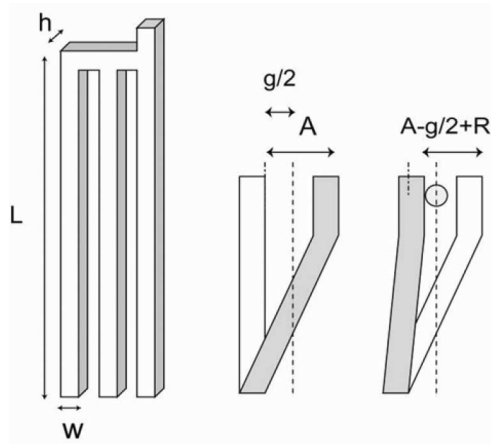

Fig. 3. (Left) geometry of the three-beam microgripper is depicted. (Right) illustration of a single arm with the actuation A, and an arm which is blocked by the other arm, and an object of radius R.

implies that heat-induced damage of the object must be considered as well.

The layout, however, enables the microgrippers to operate also by electrostatic actuation, i.e., by applying a voltage across the two three-beam arms. With electrostatic actuation, the microgripper does not heat up; but the gripping force and deflection range are lower. Even though electrostatic actuation does not cause a short between the arms due to the native oxide present on the gripper arms, care has to be taken when gripping conducting samples. The tradeoff between a high gripping force and a low temperature implies that careful consideration has to be given to both the microgripper design and the mode of operation.

B. Actuation and Gripping Force Required to Break off a Carbon Nanotube

In order to align to and break off a vertically aligned, multiwalled carbon nanotube, such as presented by Carlson *et al.* [15], the gap g between the gripper arms must be large enough to conveniently align the end-effectors to the carbon nanotube. Based on practical experience, this requires at least $g = 1$–$2\ \mu$m, which is also a gap size that can be manufactured reliably with photolithography.

In addition, each arm should be capable of not only closing to half the gap, $g/2$ (see Fig. 3), but also, further to increase the gripping force. If the gap can only barely be closed, no gripping force is available for manipulation. A large actuation combined with a large rigidity of the actuator is needed to eventually apply a large gripping force to a seized object.

When the microgripper is holding a carbon nanotube of radius R with zero gripping force, the free actuation of each arm is exactly $g/2 - R$ (see Fig. 3). The gripping force is defined here as the spring constant, k, multiplied by the overhead actuation $\Delta A = A - (g/2 - R)$ (see Fig. 3) still available when the gap is holding a nanotube

$$F_{\text{grip}} = k\left(A - \frac{g}{2} + R\right). \tag{1}$$

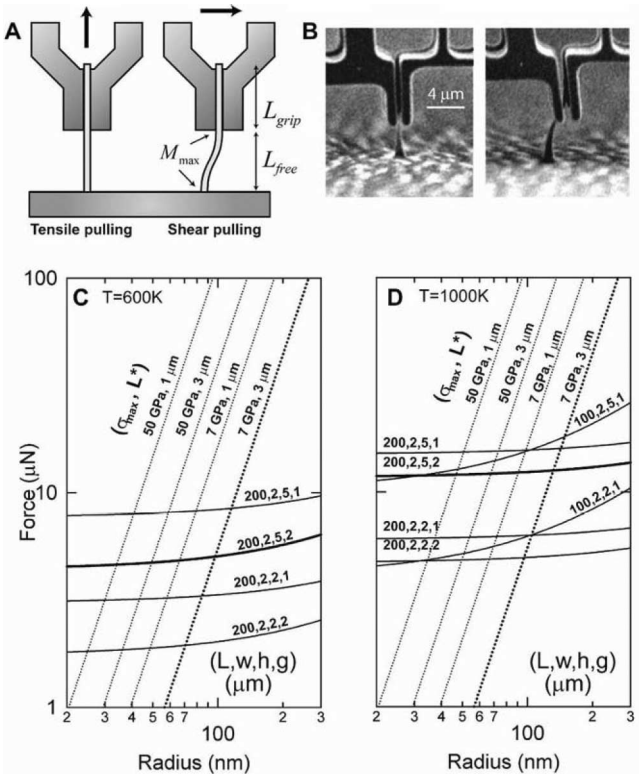

Fig. 4. (A) Illustration of tensile and shear pulling. (B) SEM images of electrothermal micrograpper picking carbon nanotubes with tensile and shear pulling, respectively. (C) Available (full lines) and required (dotted lines) gripping force versus CNT radius for breaking off CNTs (weak and strong) by shear pulling at $T_{\max} = 600$ K for different micrograpper geometries. (D) $T = 1000$ K (curves for tensile pulling not shown).

By bending a cylindrical CNT as a cantilever (one end fixed, one end free), it is possible to break it at the base where the stress and also the maximal bending moment $M_{\max}$ will be located. The bending moment $M(x)$ is related to the radius of curvature R_{curv} and the deflection $u(x)$ through the beam equation, $R_{\text{curv}}^{-1} = u''(x) = -M(x)/EI$, where E is the Young's modulus of the nanotube and $I = \pi R^4/4$ is the cylindrical plane moment of inertia. For small curvatures, we get $R_{\text{curv}} = RE/\sigma$, which then allows us to the express the maximum bending moment as

$$M_{\max} = \frac{\pi R^3 \sigma_{\max}}{4}. \tag{2}$$

A vertically aligned CNT can be detached using a micrograpper either vertically (*tensile pulling*) or laterally (*shear pulling*). These two modes are illustrated in Fig. 4(A), and shown as SEM images of a micrograpper picking up a carbon nanotube in Fig. 4(B). As discussed in a previous study [13], [15], shear pulling is much more effective than tensile pulling for nanotubes/nanowires. If the micrograpper is holding the CNT firmly, the CNT will be clamped at one end and guided at the other, which according to [16] gives the relationship: $M = FL_{\text{free}}/2$, where L_{free} is the free length of the rod. With F_{bend} as the force required to bend the CNT to the breaking point, we get: $F_{\text{bend}} = 2M_{\max}/L_{\text{free}}$.

To bend the CNT into a vertical position, as shown in Fig. 4, the left and right end-effector surfaces with length L_{grip} must generate a moment equal to the bending moment of the nanotube $M_{\max}$, preventing the CNT from forcing the jaws open. This requires a force, $F_{\text{twist}} = M_{\max}/L_{\text{grip}}$. An estimate of the total required force can be done by adding the two contributions, F_{bend} and F_{twist}

$$F_{\text{shear}} = \frac{\pi R^3 \sigma_{\max}}{4}\left(\frac{2}{L_{\text{free}}} + \frac{1}{L_{\text{grip}}}\right) \tag{3}$$

which can be evaluated without knowing the Young's modulus. The spring constant of the three-beam micrograpper is given by $k = 11E_{\text{gripper}}hw^3/(4L^3)$ [14], where E_{gripper} is the Young's modulus of the micrograpper, and h, w, and L the height, width, and length of the gripper arms, respectively. The actuation as a function of the maximum allowed temperature $\Delta T_{\max} = T_{\max} - 300$ K in actuation mode 3 (see Fig. 2), can be written as [14]

$$A_3 = \frac{\alpha L^2 \Delta T_{\max}}{18w} \tag{4}$$

where α is the thermal expansion coefficient. The expression for mode 2 can be found to be $A_2 = (4/3)A_3$. There will almost always be a maximum allowed temperature in a given manipulation experiment to avoid damage to the object or the micrograpper. Clearly, this means that the melting point of silicon, around 1700 K, must not be exceeded. Both SCS and polycrystalline silicon, however, undergo plastic (irreversible) deformation at lower temperatures than the melting temperature. At the stress levels applied during actuation, the transition from the elastic to the inelastic regime for polycrystalline silicon occurs at around 1050 K [17], while plastic transformations start to occur at around 1200–1300 K for SCS [18].

Furthermore, few nanostructures can sustain temperatures above 1000 K without damage. Although structurally perfect single-walled CNTs have a melting point exceeding 4800 K [19] and a premelting point of 2600 K for CNTs with Stones–Wales defects [19], previous experiments have shown that operating temperatures much larger than the temperature reached during the PECVD growth (around 1100–1200 K) can lead to changes in the CNT structures [19]. Here, we take 1000 K to be the maximum temperature for CNT manipulation, as long as the experiments are done in vacuum; in air, the CNTs may oxidize at much lower temperatures.

In Fig. 4 the required gripping force F_{shear} (dotted lines) is plotted for carbon nanotubes/ nanowires with yield strengths of 7 GPa and 50 GPa, representing medium-strength CNTs and high-strength CNTs, respectively [20]–[22]. A yield stress of 7 GPa is also roughly representative of plasma-enhanced chemical vapor deposition (PECVD) grown CNTs with structural defects [20]–[22]. In Fig. 4(C), curves both for short ($L^* = 1$ μm) and long ($L^* = 3$ μm) CNTs are shown, where $L^* = L_{\text{free}} = L_{\text{grip}}$.

The available force (full lines) calculated from (3) is plotted for $T_{\max} = 600$ K in Fig. 4(C) and $T_{\max} = 1000$ K in Fig. 4(D). Each curve is labeled with the geometric parameters, (length, width, height, and gap) of the micrograpper. Micrograppers with

lengths $L = 100$ and 200 μm, width 2 μm, heights 2 and 5 μm, and gap size 1 and 2 μm are plotted.

As an example, Fig. 4(C) predicts that weak ($\sigma_{\max} = 7$ GPa) CNTs with radii of up to 90 nm can be picked up by shear pulling, using a microgripper with dimensions: $L = 200$ μm, $w = 2$ μm, $h = 5$ μm, and $g = 2$ μm (heavy line).

From the curves, several observations can be made. 1) The shorter microgrippers with a gap size of 1 μm provide the largest force at 1000 K, but cannot close at 600 K, hereby not producing a gripping force. With a gap of 2 μm, the shorter microgrippers cannot close at all, and hence do not appear in any of the graphs; 2) At low temperature, $T = 600$ K, short, strong CNTs (50 GPa, 1 μm) with radii above 40 nm are not possible to break off even with the strongest microgrippers; 3) Increasing the height of the microgripper arms from 2 to 5 μm significantly improves the gripping force at both temperatures.

In a previous study by Molhave and Hansen [14], three-beam microgrippers made of gold had a width of 2 μm and a height of 1 μm. Gold has a thermal expansion coefficient of 14.2×10^{-6} K^{-1}, which is three to four times larger than silicon 2.5×10^{-6} K^{-1} [23], while the melting point of gold ($\sim$1340 K) is not far from that of silicon ($\sim$1700 K). As a result, the actuation at maximum and intermediate temperatures is considerably smaller for Si, which must then be compensated by increasing the height of the microgripper.

This also reduces the out-of-plane bending, which was a serious problem for the small-aspect ratio microgrippers [14].

Thus, by keeping the beam width and gap size at the photolithographic limit, $w = 2$ μm, a change of the height to 5 μm increases the out-of-plane spring constant $k_{\rm op}$ by a factor of 125 according to $k_{\rm op} \propto wh^3/L^3$, while providing a reasonable gripping force. With a length of 200 μm, the microgripper can operate over a large temperature range.

C. Finite-Element Simulations of Shear Pulling: How to Break off a Nanotube

It is crucial that the nanotube breaks near the base and not near the microgripper, since retaining the free end is necessary for further handling. In the aforesaid calculations of a cylindrical nanorod, the maximum moment is obtained both at the base and at the microgripper simultaneously; hence, there is equal probability of the nanotube breaking at either point.

So far, we have assumed that the carbon nanotube is cylindrical, and that the microgripper is completely closed. In practice, carbon nanotubes and nanowires are often tapered [15]. The shear pulling method was analyzed using the finite-element analysis program COMSOL. Tapered and cylindrical nanorods with a diameter of 250 nm near the lower edge of the end-effector were modeled with 6000–10000 mesh elements. The Young's modulus of the PECVD-grown multiwalled CNTs is expected to be within 0.1 and 1.0 TPa [20]–[22], [24] depending on the precise internal structure, while the yield strength is roughly 1–10 GPa [20]–[22]. In the calculations, the Young's modulus was set to 0.75 TPa. In Fig. 5(A), shear pulling of a cylindrical nanorod is shown, where a lateral deflection of 250 nm results in a stress of 18 GPa both at the base and at the lower edge of the end-effector, as expected. In the case of a tapered nanorod, Fig. 5(B), the stress is much lower at the base, which inevitably leads to breaking near the end-effector. Fig. 5(C) indicates how this situation can be avoided; a single end-effector applies a point force of 15 μN laterally, i.e., $L_{\rm free} = 3$ μm above the surface, at the lower edge of the end-effector. This generates a stress of 8 GPa at the base with almost no stress at the end-effector contact point. However, using a single end-effector, the nanotube is likely to be lost after breaking. With an increase of the applied force from 15 to 25 μN, and an oppositely directed force of just 5 μN to hold the nanorod, a stress of 8 GPa is reached near the base of the tapered nanorod, while the stress at the end-effector is significantly lower.

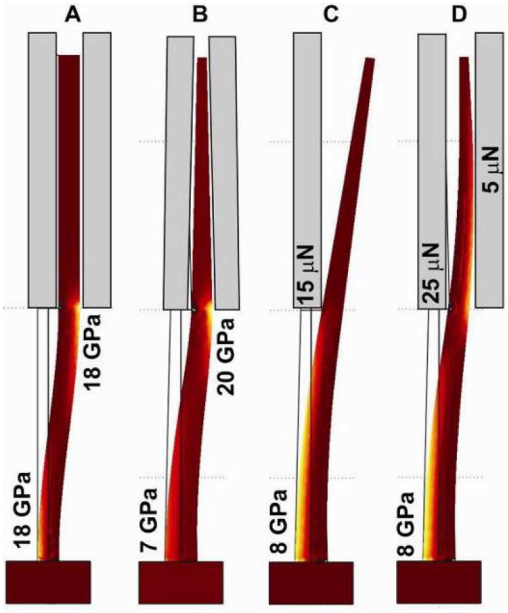

Fig. 5. (A) Cylindrical nanorod held in a firm grip. (B) Tapered nanorod held in a firm grip. (C) Tapered nanorod pushed by single end-effector. (D) Tapered nanorod held in a loose grip.

Therefore, if the tapered nanotube is only loosely held, the radius of curvature is reduced strongly near the end-effector, which shifts the point of maximum stress from the end-effector to the base. In experiments, allowing the nanotubes to force the gap to open slightly will then cause the nanotubes to consistently break off near the base.

III. Microfabrication of Microgrippers

The microgrippers are fabricated using commercial single-crystalline silicon-on-insulator (SOI) wafers as well as in-house fabricated polycrystalline wafers (pSOI), in both cases with a 5-μm device layer and a 1-μm buried oxide (SiO_2).

To be able to fully control thickness, homogeneity, and doping level in a fast and affordable manner, we used pSOI as an alternative to commercially available SOI wafers. The pSOI wafers were fabrication from single polished silicon wafers. A 1-μm thermal oxide was grown followed by low-pressure chemical vapor deposition (LPCVD) of a 5-μm-thick boron-doped polycrystalline silicon and subsequent anneal. Since the LPCVD and

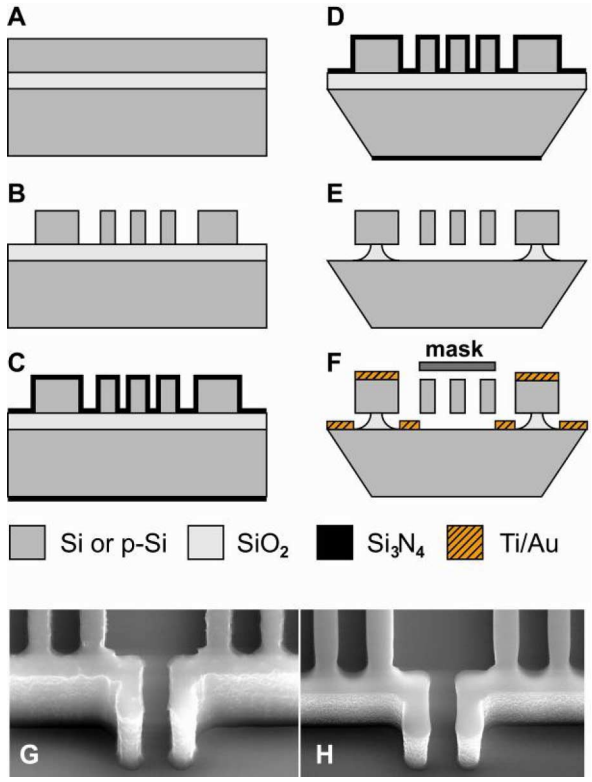

Fig. 6. (A) An SOI wafer with a 5-μm silicon device layer on top of a 1-μm SiO_2 layer. (B) The device layer is patterned using photolithography and RIE. (C) The front and backside of the wafer is covered with silicon nitride. (D) The backside is patterned using photolithography and RIE and the carrier wafer is etched from the backside using KOH. (E) The silicon nitride thin film is removed in a phosphoric acid solution, and the individual microgrippers are released by bHF. (F) Metal is deposited on the electrical connection pads on the microgripper chips through a mechanical shadow mask. (G) SEM image of pSOI microgripper at step B. (H) SEM image of SOI microgripper at step B.

oxidation processes deposit material on both sides of the wafers, the polycrystalline silicon and the SiO_2 on the back side of the wafer were removed by RIE and bHF. The polycrystalline silicon device layer had a resistivity of 0.05–0.07 Ω·cm whereas the highly doped p-type silicon $\langle 1\ 1\ 1 \rangle$ device layer of the SOI wafers had a resistivity of 0.02–0.05 Ω·cm.

Fig. 6(A)–(F) illustrates the main steps in the fabrication sequence. After defining the microgrippers in the device layer by photolithography with a high aspect ratio SF_6/O_2 based reactive ion etch (RIE) process [see Fig. 6(B)], a thin conformal low-stress silicon-rich Si_xN_y layer was deposited on both sides of the wafer [see Fig. 6(C)] using LPCVD. The backside silicon nitride was patterned lithographically and used as an etch mask for anisotropic potassium hydroxide (KOH) etch of the silicon carrier wafer with the buried SiO_2 as an etch stop [see Fig. 6(D)]. The silicon nitride was removed in phosphoric acid, and finally the microgripper structures were released with a buffered hydrofluoric acid (bHF) etch of the SiO_2 [Fig. 6(E)]. In order to be able to electrically contact the microgrippers by wire bonding, a thin film of titanium and gold was deposited on the electrical connections pads, with a mechanical shadow mask protecting the microgrippers [Fig. 6(F)]. The backside mask was designed to provide the microgripper chips with a bevelled lead such that the chips could be easily released from the wafer. The bevel lead defines the cleavage point and reduces the force necessary to remove the chips such that the microgrippers are not damaged when released using a standard tweezer [25].

The polysilicon surface roughness was measured to be in the 0.1–0.2 μm range using scanning laser confocal microscopy and atomic force microscopy. However, this film roughness did not result in significant side edge roughness as illustrated in Fig. 6(G) and (H). On the other hand, the device layer thickness variation of the SOI wafers ranged from ± 0.5 to ± 1 μm on all investigated wafers, while the device layer thickness variation of the pSOI wafers consistently was below ± 0.2 μm. Large thickness variations cause a significant decrease in yield during the RIE process, cf. Fig. 6(B), due to lateral etching. Lateral etching of the silicon device layer occurs when the buried oxide is reached and the local concentration of fluorine radical increases.

Two SOI and two pSOI wafers were fabricated with 324 microgrippers on each. The total yield of probes meeting the microfabrication specifications was 60%–80% for the polycrystalline silicon microgrippers and 80%–100% for the SCS microgrippers. In this paper, we have chosen to present two representative microgrippers of each material.

IV. Characterization and Manipulation Results

Three experimental setups were used to characterize and test the performance of the fabricated structures. 1) A setup operating in ambient air based on a high-magnification optical lens system with a long working distance. This system tracks the deflection of microgripper arms as a function of actuation voltage using a combination of image recognition, filtering, and averaging of the live frame-grabbed video images [7]. The noise level of deflection measurement can be as low as 2 nm, and the variation between subsequent actuation curves is typically 7–20 nm. 2) A system consisting of a combination of a Kleindiek 3-axis micromanipulator and a Physik Instrumente 3-axis nanopositioning stage, installed in a LEO (SEM). This system provides around 10 nm resolution both in manipulation and vision [15]. 3) A system consisting of a combination of a SmarAct 13-axis manipulation system (four *xyz* units and one rotary unit), installed in a JEOL 5900 conventional (high vacuum) (SEM). Imaging using the secondary electron signal provided an image resolution of typically 10 nm in lateral image resolution. Using working distances of $\sim$20 mm provided large depths of field of up to $\sim$500 μm. In-chamber manipulation could be carried out with subnanometer resolution in mechanical positioning and manipulation.

A. Actuation Characteristics

Fig. 7(A) shows the gap change versus bias voltage of an SCS microgripper, for each of the modes 1–4 shown in Fig. 2. The gap change is roughly twice the actuation of each individual arm. The inset shows the gap change for opening (mode 5) and closing (mode 2) as a function of bias voltage. The bias voltage was kept below 20 V for all actuation measurements to avoid permanently deforming or damaging the microgrippers.

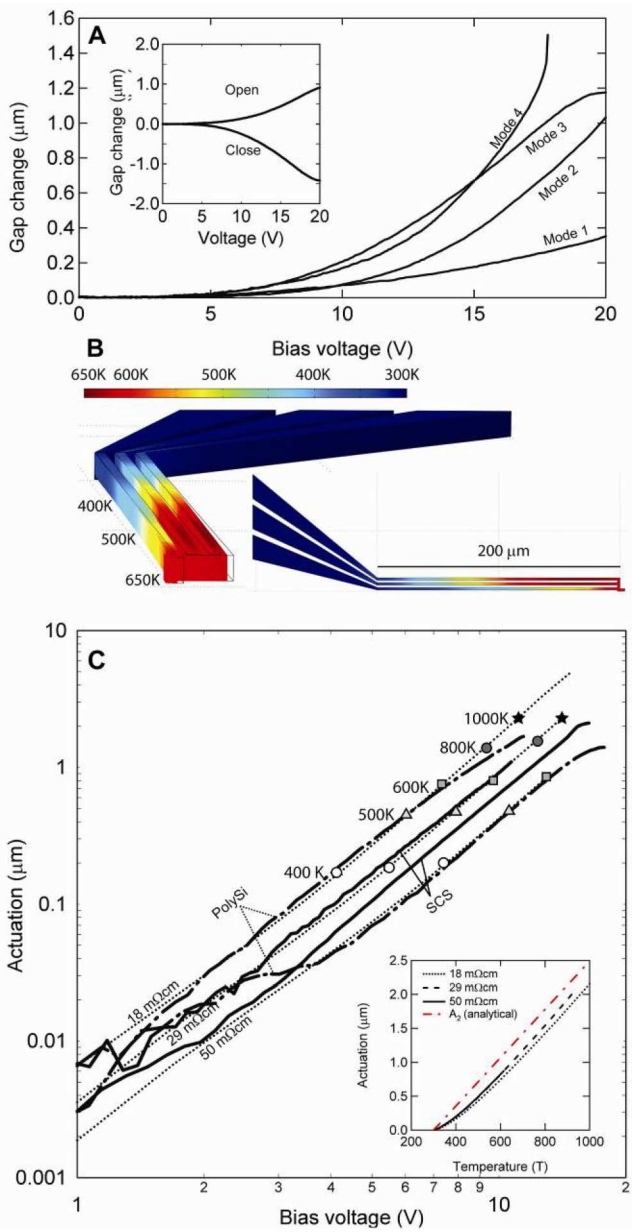

Fig. 7. (A) Total gap change Δg measured in ambient conditions between two end-effectors for four actuation modes 1–4. The inset shows the mode 2 (close) and mode 5 (open). (B) The finite element model of the actuator shown from the front and from the top, with the temperature color coded from 300 (blue) to 650 K (red). The bias voltage is 16 V, and the resistivity is 50 mΩ·cm. (C) Mode 2 actuation curves for two SCS and two poly-Si microgrippers, compared to three finite-element-simulated actuation curves for an electrical resistivity of 18, 29, and 50 mΩ·cm. The inset shows the actuation as a function of temperature for the three finite-element simulations as compared to the analytical expression.

The actuation is smallest for the purely electrostatic mode 1, and largest for the combined electrostatic and electrothermal mode 4, where electrostatic snap-in is experienced at 18 V. A slight saturation of the mode 3 actuation curve is observed at 1.2 μm. Typically, such saturation behavior can be associated with buckling [26] or plastic deformation [27].

End-effector deflection as a function of bias voltage for two polycrystalline silicon (poly-Si) and two SCS microgrippers out of 30 devices is shown in Fig. 7(C) as full lines. The poly-Si actuation curves are considerably higher than the SCS for the same voltages, due to the lower resistivity. The maximal actuation varied by a factor of 2 for the characterized devices, most likely due to process variations of the beam width. The curves are plotted as a function of the estimated voltage drop at the base of the beams by subtracting the serial resistance from the bonding pads to the actuators. The inset shows the actuation as a function of temperature for the three finite-element simulations, compared to the analytical expression for mode 2.

For comparison with experiment, finite-element calculations (Fig. 7(B)) were performed with COMSOL for a range of values of the initial resistivity, of which four are shown in the figure: 18 mΩ·cm, 29 mΩ·cm, and 50 mΩ·cm. We have not distinguished between SCS and pSi in the calculations; for such high doping levels as in our devices, the resistivity of poly-Si approaches that of SCS [28]. We use the thermal dependence of the resistivity similar to that found by Deladi *et al.* [29] for polycrystalline silicon with a resistivity of 23 mΩ·cm, comparable to the 20–50 mΩ·cm of the SCS actuators and 50–70 mΩ·cm of the poly-Si microgrippers. The temperature dependence of the thermal conductivity [30] and the thermal expansion coefficient [31] for SCS were used as well, following Deladi *et al.* [29].

The boundary conditions corresponding to mode 2 were selected, i.e., the outer beam is set to a potential V, the center beam is set to ground, and the inner beam is set floating. To properly model the temperature distribution near the base, 50×20 μm^2 fixed silicon contact areas located on top of 1 μm of SiO_2 were included. The temperature was fixed to 300 K at the bottom of the SiO_2 layer; the poor thermal conductivity of SiO_2, allows for the temperature in the device layer to drop to 300 K over 5–10 μm from the base of the actuator in a realistic way.

Since the actuation measurements were performed in ambient conditions, heat loss to the surrounding air was taken into account by introducing a convection term in the calculation of the thermal distribution, while the heat loss due to radiation in electrothermal actuation is minor even at very high temperatures [26].

The actuation curves for the four devices (poly-Si: thick, dashed lines, SCS: thick, full lines) as well as the simulations (thin, dotted lines) all follow a power law, $A \propto V^{\beta}$, with the exponent $\beta = 2.5$–2.7, differing from the parabolic actuation, $\beta = 2$, predicted analytically for temperature-independent thermal conductivity, electrical resistivity, and thermal expansion coefficient [14].

As indicated by the analytical expression for mode 3 (4), Fig. 7(c) shows a consistent relationship between the maximal end-effector temperature and the actuation for the simulations, which is independent of the resistivity. For example, the actuation at $T = 500$ K is close to 0.5 μm for all three investigated values of the electrical resistivity.

The simulations suggest that the end-effectors reach the half-gap, $g/2 = 1$ μm, at a temperature of around $T = 600$–700 K, and an actuation of 2 μm, at the maximum allowed temperature of 1000 K. This is roughly in accordance with (4), which for mode 2 gives $A_2 = (4/3)\alpha L^2 \Delta T_{\max}/18w = 2$ μm, as also shown in the inset of Fig. 7(C). Despite the analytical formula not taking the thermal dependence of the material parameters or

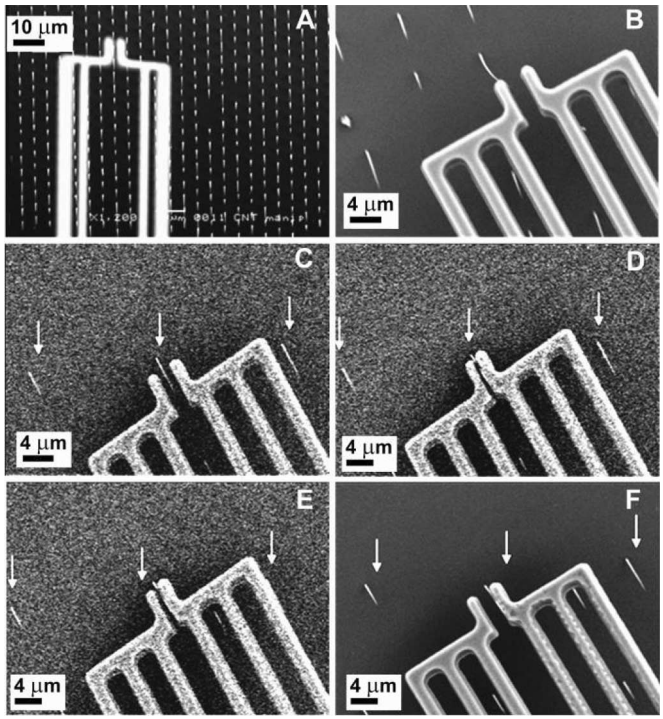

Fig. 8. Pick-and-place sequence for CNs from a 2-D ordered array using a 3-beam electrothermal silicon microgripper. The arrows indicate the position of the CNs, which are spaced by 10 μm. (A) CN ordered array and microgripper. (B) The microgripper and the CN array are brought in close contact to each other. (C) The microgripper is aligned to the CN. (D) The microgripper is closed by applying a bias voltage of 20 V. (E) The microgripper and the sample are moved sideways to detach the CN. (F) After opening the gap, the CN adheres to one of the end-effectors.

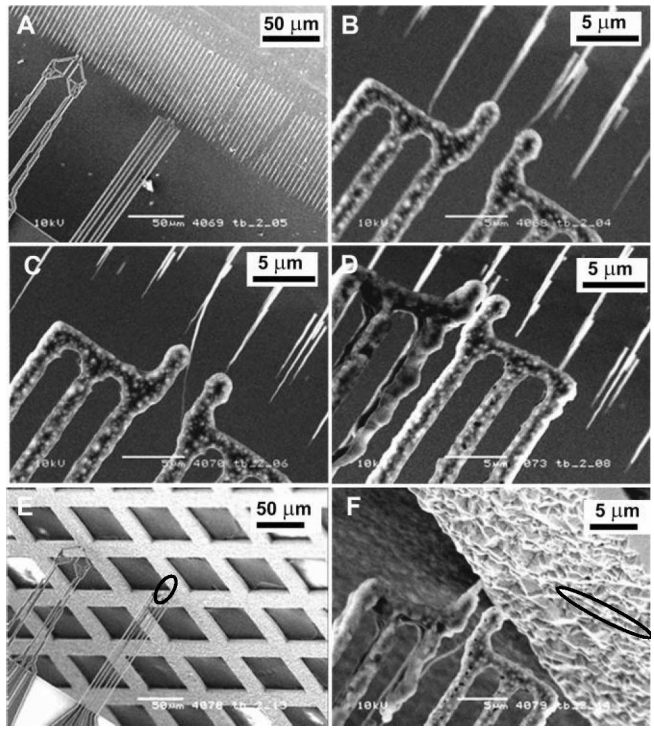

Fig. 9. Pick-and-place sequence for CNs from a 2-D ordered array using a 3-beam electrothermal polycrystalline silicon microgripper. (A) CN-ordered array with two microgrippers. (B) The three-beam microgripper and the CN array are brought in close contact to each other. (C) The microgripper is aligned to the CN and the height is adjusted such that the CN and the microgripper are in the same focal plane. (D) The microgripper is closed by applying a voltage of 20 V. The microgripper and the sample are then moved sideways to detach the CN using shear pulling. (E) The microgripper holding the gripped CN (marked by a circle) is moved toward a TEM grid. (F) The CN (marked by a circle) is released from the microgripper and placed onto the TEM grid.

the heat loss due to the surrounding air into account, it appears to give sufficiently accurate rough estimates, such as in Fig. 4. The actuation of the microgrippers in air and vacuum has only shown a minor difference.

B. Nanomanipulation Using SCS Microgrippers

An *in situ* manipulation system in an SEM, such as system II or III can be used to pick CNTs from an ordered vertical array with a microgripper and place on various substrates and devices either for characterization of the CNTs themselves or as components in various nanodevices and circuits. Figs. 8 and 9 show picking sequences of manipulation attempts from ordered arrays of carbon annotubes. Although frequently termed CNTs, large CVD-grown nanostructures are often only partly graphitized and only partly hollow, and may contain residues of the catalytic material. To steer clear of a discussion on whether the investigated structures are CNTs or carbon nanofibers (CNFs), we refer to these as CNs in the following.

In the following manipulation experiment, system II was used. First, a substrate with CNs having a diameter of about 200 nm and a length of 6–8 μm [Fig. 8(A)] and an SCS microgripper (200 μm long, 5 μm high, and 2 μm wide) are brought into close proximity [Fig. 8(B)] and into the field of view in the SEM. The microgripper is then moved such that it could grab a CN by the base [Fig. 8(C)], and closed around the CN. A large force is then applied to the microgripper and translated in order to pull off the CN, by shear pulling [Fig. 8(D)]. In Fig. 8 bottom middle, the CN has been released from the growth substrate and the microgripper is free to move the CN away. When the microgripper is opened to release the CN [Fig. 8(F)], the CN is seen adhering to the sidewall of the microgripper. Due to the rigidity and strong fixture to the surface, and the mechanical flexibility of the 3-beam microgrippers, this experiment was only successful in a few cases; in most cases, the CNs were bent but not broken. We were not able to break off any CN by tensile pulling (vertically), regardless of the gripping force, as predicted by Carlson *et al.* [15]. So far, the smallest diameter CN that we have been able to grab has a diameter of 50 nm.

C. Nanomanipulation Using Polycrystalline Silicon Microgrippers

Fig. 9 shows a pick-and-place sequence where a CN is transferred from the aligned array used previously (Section IV-B) onto a TEM grid for further analysis. System III was used in these manipulation experiments. First, a substrate with the array of CNs described earlier [Fig. 9(A)] and a polycrystalline silicon microgripper (150 μm long, 5 μm high, and 2 μm wide) are brought into close proximity and into the field of view in the

SEM (B). The microgripper is then aligned such that it could grab a CN by the base (C), and closed around the CN (D). The gripper is then translated in order to pull off the CN by shear pulling. The CN has been released from the growth substrate, and the microgripper holding the CN is moved toward a TEM grid (E). The microgripper is then opened to release the CN [Fig. 9(F)] and the CN is seen adhering to the sidewall of the TEM grid. Due to the shorter length of the microgripper compared to the gripper used in Section IV-B, the CNs could be broken off the growth substrate by shear pulling with a reasonable reliability.

V. Discussion

Silicon microgrippers were used for pick-and-place nanomanipulation of CNs. Compared to an earlier study [14], the higher aspect ratio limits out-of-plane deflections, while delivering sufficient force to detach carbon nanotubes and fibers up to several hundred nanometers in diameter. The ability to operate a microgripper in several modes increases the effective actuation range and provides flexibility in matching the specific constraints of a certain manipulation experiment, for instance, by combining electrostatic and electrothermal operation mode.

A simple analysis of the force requirements when detaching cylindrical CNs with a lateral motion of the gripper (shear pulling) showed that detachment at a moderate temperature ($T = 600$ K) where neither carbon nanofibres or microgripper is likely to be damaged, favors longer grippers (200 μm) with a high aspect ratio (2 μm wide and 5 μm long). Microgrippers with these dimensions should be able to detach CNs with moderate yield strength (7 GPa) with a radius up to 100 nm and strong CNs (50 GPa) with a radius up to 50 nm. At a higher operating temperature ($T = 1000$ K) shorter grippers can close, which generates higher gripping forces due to the increased spring constant. A more detailed analysis of the detachment of cylindrical and tapered CNs, using finite-element calculations, indicated that a slight opening of the microgripper reduces the radius of curvature near the microgripper significantly, which will shift the position of highest stress and thereby the point of detachment closer to the base rather than near the gripper.

The microfabrication process for defining 5 μm tall, 200 μm long 3-beam microgripper structures in both poly- and SCS was described. The sidewalls of the processed microgrippers are not completely smooth. This can be an advantage since a rough gripping surface can reduce the stiction between the CN and the microgripper. The processed polycrystalline silicon surfaces generally showed a much rougher morphology than SCS surfaces (see Figs. 8 and 9) since they are composed of grains of different crystal orientation. Although no systematic difference in the RIE-etched sidewall roughness was observed for poly-Si and SCS, perfectly vertical sidewalls were, in general, difficult to achieve consistently. This may influence the ability to hold the CN securely, and also in some cases created considerable variation in the force required to detach the CNs. The actuation properties (deflection as a function of bias voltage) of poly-Si and SCS microgrippers showed good agreement with finite-element calculations.

Two examples of nanomanipulation were presented. In accordance with the simple analysis, manipulation experiments showed that CNTs with a diameter of 100 nm could be picked with the 200-μm-long microgrippers. Using a shorter microgripper (150 μm) made of poly-Si, morphological changes were observed during operation, indicating that an operating temperature in the range of 1000 K is necessary to close the gap. As predicted by the simple analysis, the shorter microgripper showed better performance in terms of gripping force, at the cost of a higher operating temperature.

The microgripper design could be further improved by focusing on shear pulling of nanostructures. If one of the arms is made rigid, such that the rigid arm breaks the nanotube, and the other more flexible arm holds the carbon nanotube after pushing, as demonstrated by Carlson *et al.* [15], the ability to open makes it possible to narrow the gap (increase force) while still making it possible to align the gap to small CNs. If a tapered CN is only loosely held, the radius of curvature is reduced strongly near the end-effector, which shifts the point of maximum stress from the end-effector to the base. In experiments, allowing the CNs to force the gap to open slightly will then cause the CNs to consistently break off near the base, thereby avoiding CNs breaking at the point of the microgripper end-effectors.

The 3-beam microgripper design can also be used for force sensing by taking advantage of the piezoresisitve response through a built-in Wheatstone bridge, as shown for Au grippers in a previous study [13]. Since silicon has a much higher piezoresistive gauge factor than gold, the possibility of incorporating a sensitive lateral force detection scheme with manipulation could be used to better adjust the gripping force and thereby provide a better control of the detachment process. Such a scheme could be highly useful for reducing the need for simultaneous monitoring with SEM, which will be a complicating factor in the realization of a fully or partly automated assembly scheme based on microgrippers.

Acknowledgment

The authors would like to thank the Engineering Department at the University of Cambridge, U.K., for supplying arrays of vertically aligned carbon nanotubes.

References

[1] C. J. Kim, A. P. Pisano, R. S. Muller, and M. G. Lim, "Polysilicon microgripper," *Sensors and Actuators A*, vol. 33, no. 3, pp. 221–227, 1992.
[2] *Nascatec*, Nascatec GmbH, Stuttgart, Germany, 2007.
[3] *Zyvex*, Zyvex Corporation, Richardson, TX, 2007.
[4] *FemtoTools*, FemtoTools GmbH, Zurich, Switzerland, 2007.
[5] P. Kim and C. M. Lieber, "Nanotube nanotweezers," *Science*, vol. 286, no. 5447, pp. 2148–2150, 1999.
[6] P. Boggild, T. M. Hansen, C. Tanasa, and F. Grey, "Fabrication and actuation of customized nanotweezers with a 25 nm gap," *Nanotechnology*, vol. 12, no. 3, pp. 331–335, 2001.
[7] K. Molhave, T. M. Hansen, D. N. Madsen, and P. Boggild, "Towards pick-and-place assembly of nanostructures," *J. Nanosci. Nanotechnol.*, vol. 4, no. 3, pp. 279–282, 2004.

[8] M. Yu, M. J. Dyer, G. D. Skidmore, H. W. Rohrs, X. Lu, K. D. Ausman, J. R. V. Ehr, and R. S. Ruoff, "Three-dimensional manipulation of carbon nanotubes under a scanning electron microscope," in *Proc. Nanotechnol.*, 1999, pp. 244–252.
[9] T. Fukuda, F. Arai, and L. X. Dong, "Assembly of nanodevices with carbon nanotubes through nanorobotic manipulations," *Proc. IEEE*, vol. 91, no. 11, pp. 1803–1818, Nov. 2003.
[10] L. X. Dong, F. Arai, and T. Fukuda, "Nanoassembly of carbon nanotubes through mechanochemical nanorobotic manipulations," *Jpn. J. Appl. Phys., Part 1—Reg. Papers Short Notes Rev. Papers*, vol. 42, no. 1, pp. 295–298, 2003.
[11] S. Fatikow, *Automated Nanohandling by Microrobots*. New York: Springer, 2008.
[12] K. B. K. Teo, M. Chhowalla, and G. A. J. Amaratunga, "Uniform patterned growth of carbon nanotubes without surface carbon," *Appl. Phys. Lett.*, vol. 79, no. 10, pp. 1534–1536, 2001.
[13] K. Molhave, T. Wich, A. Kortschack, and P. Boggild, "Pick and place nanomanipulation using microfabricated grippers," *Nanotechnology*, vol. 17, pp. 2434–2441, 2006.
[14] K. Molhave and O. Hansen, "Electro-thermally actuated microgrippers with integrated force-feedback," *J. Micromech. Microeng.*, vol. 15, no. 6, pp. 1265–1270, 2005.
[15] K. Carlson, K. N. Andersen, V. Eichhorn, D. H. Petersen, K. Mølhave, I. Y. Y. Bu, K. B. K. Teo, W. I. Milne, S. Fatikow, and P. Bøggild, "A carbon nanofibre scanning probe assembled using an electrothermal microgripper," *Nanotechnology*, vol. 18, no. 34, pp. 345501-1–345501-7, 2007.
[16] W. C. Young, *Roark's Formulas for Stress & Strain*. New York: McGraw-Hill, 1989.
[17] W. N. Sharpe *et al.*, "Tensile testing of MEMS materials—recent progress," *J. Mater. Sci.*, vol. 38, no. 20, pp. 4075–4079, 2003.
[18] V. M. Glazov and A. S. Pashinkin, "The thermophysical properties (heat capacity and thermal expansion) of single-crystal silicon," *High Temp.*, vol. 39, no. 3, pp. 443–449, 2001.
[19] K. Zhang, G. M. Stocks, and J. Zhong, "Melting and premelting of carbon nanotubes," *Nanotechnology*, vol. 18, pp. 285703–286708, 2007.
[20] J. P. Salvetat, A. J. Kulik, J. M. Bonard, G. A. D. Briggs, T. Stockli, K. Metenier, S. Bonnamy, F. Beguin, N. A. Burnham, and L. Forro, *Adv. Mater.*, vol. 11, pp. 161–165, 1999.
[21] M. F. Yu *et al.*, "Strength and breaking mechanism of multiwalled carbon nanotubes under tensile load," *Science*, vol. 287, no. 5453, pp. 637–640, 2000.
[22] M. F. Yu, O. Lourie, M. J. Dyer, K. Moloni, T. F. Kelly, and R. S. Ruoff, "Tensile loading of ropes of single wall carbon nanotubes and their mechanical properties," *Phys. Rev. Lett.*, vol. 84, no. 24, pp. 5552–5555, 2000.
[23] V. M. Glazov and A. S. Pashinkin, *The Thermophysical Properties (Heat Capacity and Thermal Expansion) of Single Crystal Silicon*. New York: Springer, 2001.
[24] S. Fatikow, S. Kray, V. Eichhorn, and S. Tautz, "Development of a nanohandling robot station for nanocharacterization by an AFM probe," in *IEEE Mediterr. Conf. Control Autom. (MED)*, Ancona, Italy, 2006, pp. 1–6.
[25] D. H. Petersen, "High aspect ratio silicon beam fabrication and large scale nanowire integration," in *Proc. MIC*. Kongens Lyngby, Denmark: Technical University of Denmark, 2006.
[26] R. Hickey, D. Sameoto, T. Hubbard, and M. Kujath, "Time and frequency response of two-arm micromachined thermal actuators," *J. Micromech. Microeng.*, vol. 13, no. 1, pp. 40–46, 2003.
[27] L. J. Li and D. Uttamchandani, "Modified asymmetric micro-electrothermal actuator: Analysis and experimentation," *J. Micromech. Microeng.*, vol. 14, no. 12, pp. 1734–1741, 2004.
[28] T. Kamins, *Polycrystalline Silicon for Integrated Circuits and Displays*, 2nd ed. New York: Springer, 1998.
[29] S. Deladi, G. Krijnen, and M. C. Elwenspoek, "Parallel-beams/lever electrothermal out-of-plane actuator," in *Microsystem Technologies—Micro- and Nanosystems—Information Storage and Processing Systems,* vol. 10. Berlin: Springer, no. 5, pp. 393–399, 2004.
[30] C. J. Glassbrenner and G. A. Slack, "Thermal conductivity of silicon + germanium from 3 degrees K to melting point," *Phys. Rev. A, Gen. Phys.*, vol. 134, no. 4A, pp. 1058–1069, 1964.
[31] Y. Okada and Y. Tokumaru, "Precise determination of lattice-parameter and thermal-expansion coefficient of silicon between 300-K and 1500-K," *J. Appl. Phys.*, vol. 56, no. 2, pp. 314–320, 1984.

Karin Nordström Andersen received her M.S. degree in physics and mathematics from Aarhus University, Denmark, in 1999 and the Ph.D. degree in the field of integrated optics from the Technical University of Denmark in 2005.

After her Ph.D. she was a Postdoctoral Fellow at the Department of Micro- and Nanotechnology at the Technical University of Denmark. She is currently a Senior Consultant. Her research has included developing tools for handling nanostructures (mainly nanotubes, nanowires, and nanofibers) and using these tools to explore the fundamental physical characteristics of such manipulation scenarios. Her present research interests include surface engineering, surface structuring, surface coatings, hydrophobic surfaces, 3-D nanostructuring, and optical surfaces.

D. H. Petersen, photograph and biography not available at the time of publication.

K. Carlson, photograph and biography not available at the time of publication.

K. Mølhave, photograph and biography not available at the time of publication.

Ozlem Sardan received the B.Sc. degree in mechanical engineering from the Middle East Technical University (METU), Ankara, Turkey, and the M.Sc. degree in mechanical engineering from the Koc University, Istanbul, Turkey, in 2004 and 2006, respectively.

Since October 2006, she is a Ph.D. student at the Department of Micro- and Nanotechnology (Nanotech) at the Technical University of Denmark (DTU). Her current research interests include design, fabrication and characterization of microactuators, nanomanipulation/assembly, and topology optimization. Ms. Sardan is a student member of the American Society of Mechanical Engineers (ASME).

A. Horsewell, photograph and biography not available at the time of publication.

Volkmar Eichhorn received his diploma in physics from the University of Oldenburg, Germany, in 2005. His thesis dealt with optical metrology measurements based on electronic speckle pattern interferometry. Since 2005 he has been working at the Division Microrobotics and Control Engineering on his doctoral thesis. His main research interest is nanorobotic handling and characterization of carbon nanotubes inside the scanning electron microscope. Therefore, he is mapping out strategies for reliable pick-and-place handling as well as nondestructive electrical and mechanical characterization of individual CNTs. Furthermore he is working on the prototypic assembly of CNT-based devices. He is head of the group "Handling and Characterization of Nanoscale Objects" and published more than 20 technical papers in books, journals, and conference proceedings.

Sergej Fatikow studied computer science and electrical engineering at the Ufa Aviation Technical University in Russia, where he received his doctoral degree in 1988 with work on fuzzy control of complex nonlinear systems.

He worked until 1990 as a Lecturer at the same university. During his work in Russia he published over 30 papers and successfully applied for over 50 patents in the area of intelligent control. In 1990 he moved to the Institute for Process Control and Robotics at the University of Karlsruhe, Germany, where he worked as a postdoctoral scientific researcher and since 1994 as Head of the research group "Microrobotics and Micromechatronics". He became in 1996 an Assistant Professor. In 2000 he accepted an Associate Professor position at the University of Kassel, Germany. A year later, he was invited to establish a new Division for Microrobotics and Control Engineering at the University of Oldenburg, Germany. Since 2001 he is a full professor in the Department of Computing Science and Head of this Division. He is also Head of Technology Cluster Automated Nanohandling at the Research Institute for Information Technology (OFFIS) in Germany. He is author of three books on microsystem technology, microrobotics, microassembly, and nanohandling automation, published by Springer in 1997, Teubner in 2000, and Springer in 2008. He also published since 1991 over 50 journal papers and over 160 conference papers on micro- and nanorobotics, nanohandling automation, and intelligent robot control. His research interests include micro- and nanorobotics, automated robot-based nanohandling in SEM, micro- and nanoassembly, AFM-based nanohandling, microactuators and microsensors, and neuro-fuzzy robot control.

Peter Bøggild received the Ph.D. degree at Copenhagen University, Denmark, in 1998 in the field of experimental low temperature physics.

He is currently an Associate Professor heading the Nanointegration research group at MIC – Department for Micro- and Nanotechnology, at the Technical University of Denmark. He has built a research group concerned with development of new nanoscale tools for manipulation and characterization of nanostructures as well as generic methods for connecting molecular nanocomponents such as carbon nanotubes with microsystems. Recently, the focus areas are 1) parallel integration (wafer-scale) methods such as in-situ growth of nanocomponents directly in Microsystems, or self-assembly using electrostatic fields; 2) automated nanorobotic manipulation systems for prototyping of nanodevices; and 3) integration of molecular electronics with mass-produced nanocircuitry.